JOURNAL OF SPACECRAFT AND ROCKETS
Vol. 34, No. 4, July–August 1997

Effect of Isolated Roughness Elements on Boundary-Layer Transition for Shuttle Orbiter

John J. Bertin*
U.S. Air Force Academy, Colorado 80840-6222
Kenneth F. Stetson†
Dayton, Ohio 45459
Stanley A. Bouslog‡
Rohr Industries, Inc., Chula Vista, California 91910
and
Jose M. Caram§
NASA Johnson Space Center, Houston, Texas 77058

A 1.75% scale model of the Shuttle Orbiter has been tested in the Mach 8 Tunnel B at the Arnold Engineering Development Center with and without isolated roughness elements. Heat flux gauges on the windward surface permitted the evaluation of heat transfer distributions and boundary-layer transition trends on the Orbiter's windward surface. The data obtained during the current program have been reviewed and compared with transition results from previous tests using both a smooth model and those with distributed roughness. Results indicated that, for many test conditions, a single, relatively small roughness element can be effective in promoting boundary-layer transition, i.e., moving transition close to the roughness element.

Nomenclature

b	= model span, 16.4 in.
$h_{\text{rat,SS}}$	= numerator is the dimensionless heat transfer coefficient for the data with the roughness element(s) at the indicated freestream Reynolds number; denominator is the dimensionless heat transfer coefficient for the data obtained on the smooth configuration at the same Reynolds number and at the same angle of attack
h_{ref}	= heat transfer coefficient obtained using the Fay and Riddell[11] relation with a 0.0175-ft-radius sphere
h/h_{ref}	= dimensionless heat transfer coefficient; recovery factor of unity
k	= height of the roughness element
L	= length of the model, 22.58 in.
M_e	= edge Mach number
Re_k	= roughness Reynolds number using flow properties at the top of the roughness element, $\rho_k U_k k/\mu_k$
$Re_{k,\text{RE}}$	= roughness Reynolds number evaluated at the isolated roughness element
$Re_{k,x=0.1L}$	= roughness Reynolds number evaluated at $x = 0.1L$
Re_x	= Reynolds number based on the local flow properties at the edge of the boundary layer and the axial coordinate
Re_θ	= momentum thickness Reynolds number
$Re_{\infty,L}$	= Reynolds number based on the freestream conditions and the model length
T_t	= total temperature
T_w	= wall temperature
x	= axial distance; see Fig. 2
x/L	= nondimensionalized axial distance
x_{RE}	= x coordinate of the roughness element
x_{tr}	= axial location of boundary-layer transition
$x_{\text{tr,s}}$	= x coordinate for transition on the smooth model
y	= lateral distance; see Fig. 2
y_{RE}	= y coordinate of roughness element
$2y/b$	= nondimensionalized lateral distance
α	= angle of attack
δ^*	= displacement thickness
δ^*_{RE}	= displacement thickness at the roughness element
θ	= momentum thickness

Introduction

SPECIFICATION of criteria that can be used to predict when boundary-layer transition would occur during the flight of any vehicle, regardless of its speed range, has been, is, and will remain a challenge to the designer. The complexity of the transition process makes it extremely difficult to develop analytical models that follow the growth of unstable disturbances until they amplify to the point that the boundary layer becomes transitional, as might be indicated by an increase in the local heat transfer rate above the level characteristic of a laminar boundary layer. Thus, the designers of a vehicle often turn to correlations based on experimental data for criteria that can be used to predict when boundary-layer transition would occur for the desired application.

The designers of the Space Shuttle Orbiter made extensive use of wind-tunnel tests to develop correlations to predict the onset of boundary-layer transition. The Orbiter's blunt nose and large angles of attack during re-entry (in the range of 30–40 deg) ensure that the flowfield will be that for a blunt body with crossflow. Transition locations determined from the heat transfer distributions obtained on a smooth model[1] served as the reference transition locations. Because the windward surface of the Orbiter is composed of a large number of thermal protection tiles, the transition criteria must include the effect of the distributed roughness arising from joints and tile misalignments. To study the effect of tile misalignment on boundary-layer transition, heat transfer data were obtained using Orbiter models in which a herringbone pattern of misaligned tiles (symmetric about the plane of symmetry) covered the windward surface of the Orbiter model up to the tangent line of the chines from $x = 0.02L$ to $0.80L$ (Ref. 2). The raised tiles, which were selected randomly,

Received Aug. 8, 1996; revision received April 4, 1997; accepted for publication April 8, 1997.

*Professor of Aeronautics, Department of Aeronautics. Fellow AIAA.
†Consultant. Associate Fellow AIAA.
‡Group Engineer, Technical Resources Department. Associate Fellow AIAA.
§Aerospace Engineer, Aerospace Flight Mechanics Division. Senior Member AIAA.

represented 20% of the tiles in the area of interest. Heat transfer data were obtained for misaligned tile heights of either 0.001 in. ($4.43 \times 10^{-5}L$) or 0.002 in. ($8.86 \times 10^{-5}L$). From these tests, it was learned that surface roughness had no measurable effect on the transition location until $Re_{k,x=0.1L} = 30$. Thus, 30 is the incipient value of $Re_{k,x=0.1L}$. The transition location moves slowly forward until $Re_{k,x=0.1L} = 110$, which is the critical value. Above this critical value, transition moves rapidly forward until $Re_{k,x=0.1L} = 180$, when transition is at its upstream-most location. Because the misaligned tiles now serve as effective tripping devices, 180 is the effective value of $Re_{k,x=0.1L}$. Using these data, a transition methodology was developed at the NASA Johnson Space Center (JSC) to make preflight assessments of the effects of surface roughness on the Orbiter boundary-layer transition.

The development flight instrumentation provided heat transfer distributions, which were used to determine the boundary-layer-transition locations from the first five flights of the Space Shuttle Orbiter, designated STS (space transportation system)-1 through STS-5. Analysis of these boundary-layer-transition data led to the conclusion "that accurate predictions of transition times can be made for the orbiter at hypersonic flight conditions by using the roughness-dominated wind tunnel data."[3] Bouslog et al.[4] reported that, for a typical re-entry, boundary-layer transition occurred 1200 s after the Orbiter passed the entry interface, at an altitude of 156,000 ft, where the freestream Mach number was approximately 8 and the freestream Reynolds number was approximately 8×10^6 (based on the vehicle length).

However, the temperature histories on certain Orbiter flights have indicated heating to the windward surface of the Orbiter well above the nominal values. Furthermore, control-surface deflections and reaction-control-jet activity have indicated unusually high moments acting on the vehicle. The anomalous behavior has been attributed to early and/or asymmetric boundary-layer transition. During the STS-28 flight, surface thermocouples indicated that transition began 900 s into the entry, when M_∞ was 18 and the altitude approximately 206,000 ft (Ref. 5). The premature onset of transition as observed during the entry of STS-28 has been attributed to two gap fillers protruding into the boundary layer.[5] During the flight of STS-50, Orbiter elevon deflections and yaw reaction-control-jet firings indicated that the vehicle experienced a yawing moment at the same time as the onset of boundary-layer transition. Surface thermocouples indicated that boundary-layer transition occurred on the right side of the vehicle 80 s before occurring on the left side. Thus, the asymmetric onset of boundary-layer transition is consistent with indications of a yawing moment at the same time.

Although these data were well within the design limits for the Shuttle Orbiter, there was concern because these measurements indicated significant deviations from the expected environment. To investigate these anomalies, two experimental investigations were conducted in 1995 to increase the understanding of the effects of isolated roughness elements on boundary-layer transition on the Orbiter. Data were obtained using a 0.0075-scale model in the Mach 6 wind tunnel at the NASA Langley Research Center.[4] The data that are discussed in the present paper were obtained in a wind-tunnel test program in which isolated roughness elements were placed at various locations on a 0.0175-scale model of the Space Shuttle Orbiter that was tested in Tunnel B of the Arnold Engineering Development Center (AEDC). Heat transfer data were obtained at a freestream Mach number of 8, with freestream Reynolds numbers, based on model length, from 1.158×10^6 to 6.800×10^6, and at angles of attack of 35, 38, and 40 deg. For a more detailed discussion of these data, the reader is referred to Refs. 6 and 7.

Experimental Program

Model

A 0.0175-scale model of the Shuttle Orbiter 29-O, per Rockwell drawing VL 70-000139, was tested in Tunnel B at AEDC in June 1995. As indicated in Fig. 1, the characteristic dimension of the Shuttle Orbiter model was its body length (L), which was 22.58 in. The wing span was 16.4 in. The body flap was set at 0-deg deflection angle. Also, note that the vertical tail and the orbital maneuvering system pods were not represented on the wind-tunnel model. Of course, because the focus of the present wind-tunnel test was the flowfield on the windward surface, the absence of these features will not affect the results.

Table 1 Configurations

S1: Reference, smooth configuration
S2: E-2 ($x_{RE} = 0.258L$, $2y_{RE} = 0.043b$, $k = 0.005$ in.) and I-2 ($x_{RE} = 0.375L$, $2y_{RE} = 0.146b$, $k = 0.006$ in.)
S3: A-2 ($x_{RE} = 0.050L$, $2y_{RE} = 0.000b$, $k = 0.004$ in.)
S5: G-2 ($x_{RE} = 0.375L$, $2y_{RE} = 0.000b$, $k = 0.006$ in.) or G-3 ($x_{RE} = 0.375L$, $2y_{RE} = 0.000b$, $k = 0.015$ in.)
S6: C-3 ($x_{RE} = 0.070L$, $2y_{RE} = 0.030b$, $k = 0.008$ in.) or C-4 ($x_{RE} = 0.070L$, $2y_{RE} = 0.030b$, $k = 0.015$ in.)
S10: J-2 ($x_{RE} = 0.575L$, $2y_{RE} = 0.000b$, $k = 0.010$ in.) and K-3 ($x_{RE} = 0.620L$, $2y_{RE} = 0.366b$, $k = 0.008$ in.)
S11: F-3 ($x_{RE} = 0.285L$, $2y_{RE} = 0.107b$, $k = 0.015$ in.)

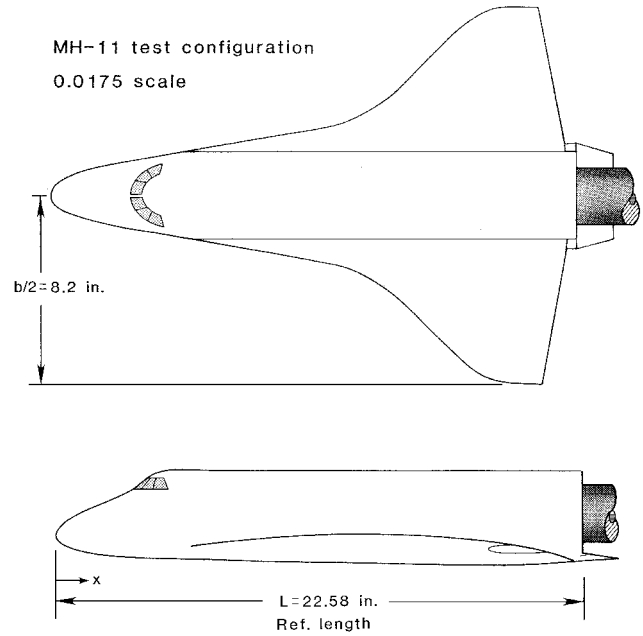

Fig. 1 Sketch of the MH-11 model.

A majority of the parts used in the fabrication of the current wind-tunnel model, which is designated MH-11, came from a model used in earlier test programs conducted in Tunnel B of AEDC. The objectives of these earlier test programs included determining the effect of randomly misaligned tiles on the boundary-layer transition criteria to be used for the re-entry of the Space Shuttle Orbiter. Therefore, for the model used in the earlier test programs,[2] which was designated MH2B, 20% of the tiles (selected at random from the first 80% of the windward surface) protuded approximately 0.0020 in. above the surrounding surface. The MH2B model was machined until the finish of the windward surface for the MH-11 model was 0.0010 ± 0.0005 in. This served as the nominal finish of the reference smooth configuration (S1) of the present test program.

The purpose of the present test program was to determine the effect of specific, discrete roughness elements on the transition of the boundary layer on the windward surface of the Space Shuttle Orbiter. Therefore, the model was designed so that one could attach roughness elements at 11 different locations on the windward surface, as shown in Fig. 2. In reality, the configurations tested employed either a single roughness element or a pair of roughness elements. A sketch of a roughness element is provided as an inset to Fig. 2. Note that, because the roughness element represented protruding gap filler, it was oriented on the model such that it was approximately 45 deg to the model centerline. The location and size of the roughness element(s) for the seven configurations for which data have been obtained are presented in Table 1. The reader can see that, for two of the configurations, S5 and S6, either one of two different height roughness elements was placed at the specified location. Two of the configurations, S2 and S10, have roughness elements at two different locations at the same time.

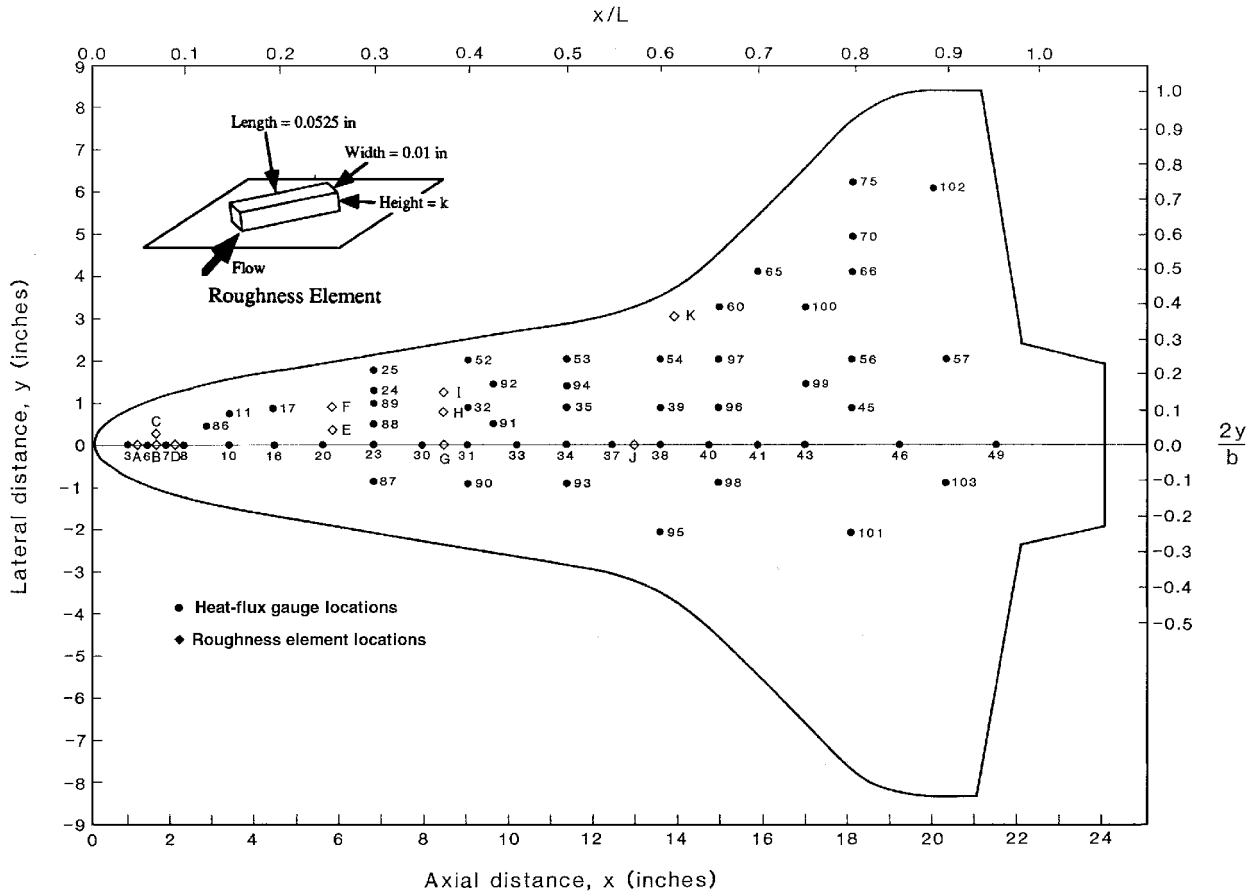

Fig. 2 Location of the heat flux gauges and the roughness elements on the model windward surface (with a typical roughness element).

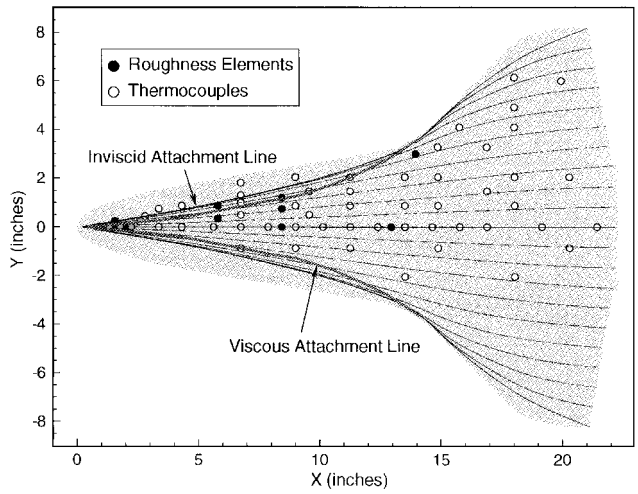

Fig. 3 Streamline patterns for an angle of attack of 40 deg, heat transfer gauges, and locations of roughness elements for the 0.0175-scale Orbiter model.

The model was instrumented with 55 coaxial heat transfer gauges, the locations of which are indicated in Fig. 2. The coaxial heat transfer gauges, which were 0.125 in. in diameter, utilized a chromel-constantan thermocouple to provide the temperature needed to determine the heat transfer rate to a point on the model surface.

The locations of the roughness elements and of the heat transfer gauges in relation to the streamlines and to the attachment lines are presented in Fig. 3. Flow inboard of the attachment line flows over the windward surface; flow outboard of the attachment line flows around the edges and onto the leeward surface. The inviscid streamlines (the fine lines of Fig. 3, bounded by the inviscid attachment line) were determined using the surface velocities as computed using an Euler code (IEC3D).[8] The viscous attachment line (a bold line of Fig. 3) represents the viscous shear stress vector at the surface of the Orbiter model, as computed using the LAURA code.[9] The computed streamlines are for the test conditions corresponding to a freestream Mach number of 8 and a Reynolds number based on the freestream conditions and on the model length of 1.9×10^6. Based on the streamline patterns, the present authors believe that the transition locations inboard of the attachment lines are not significantly affected by crossflow. Note that roughness elements C, F, and I are located near the attachment line, when the model is at an angle of attack of 40 deg. Transition at these locations may be affected by crossflow, depending on the exact location of the roughness element relative to the attachment line. Roughness element F (located at $x = 5.83$ in.) is inboard of the inviscid attachment line and outboard of the viscous attachment line. Roughness element I (located at $x = 8.47$ in.) lies on the viscous attachment line, well inboard of the inviscid attachment line.

Tunnel Test Conditions

Data were obtained in Tunnel B at AEDC at a nominal Mach number of 8 for angles of attack of 35, 38, and 40 deg. The conditions in the stilling chamber included a total pressure p_{t1} in the range 100–851 psia and a total temperature T_{t1} in the range 1235–1343°R. As a result, the Reynolds number based on the freestream conditions and the model length, i.e.,

$$Re_{\infty,L} = \frac{\rho_\infty U_\infty L}{\mu_\infty} \tag{1}$$

ranged from 1.158×10^6 to 6.800×10^6. In the presentation of the data, ReL will be used to represent the Reynolds number (based on the freestream conditions and the model length) in millions. This shorthand notation will eliminate clutter in the legends used in the graphs. In essence,

$$ReL = Re_{\infty,L} \times 10^{-6} \tag{2}$$

Measurement uncertainties are a combination of bias and precision errors. The data uncertainties for the measurements were

Table 2 Correlation parameters for boundary-layer transition in the windward pitch plane of the smooth Shuttle Orbiter

Run	Configurations	ReL	T_w/T_t	$x_{tr,s}/L$	M_e	$Re_x(\times 10^{-6})$	Re_θ	Re_θ/M_e
			Previous data: $\alpha = 30$ deg (Ref. 2)					
——	OH4A	7.004	0.400	0.55	——	1.383	——	234
——	OH4A	5.619	0.405	0.60	——	1.399	——	218
——	OH4A	4.666	0.412	0.70	——	1.402	——	216
——	OH4A	3.655	0.411	0.75	——	1.212	——	200
			Present data: $\alpha = 35$ deg					
117	S1R27	6.712	0.370	0.40	1.98	1.39	400	202
119	S1R37	5.631	0.377	0.50	2.09	1.68	441	211
121	S1R35	4.704	0.386	0.55	2.14	1.60	431	201
123	S1R39	3.748	0.385	0.65	2.25	1.68	438	195
125	S1R43	2.814	0.397	0.80	2.40	1.75	444	185
			Present data: $\alpha = 40$ deg					
116	SIR25	6.736	0.374	0.40	1.61	1.12	369	229
118	SIR29	5.613	0.370	0.50	1.69	1.34	400	237
126	SIR45	5.093	0.395	0.55	1.73	1.39	407	235
120	SIR33	4.712	0.384	0.55	1.73	1.28	392	227
122	SIR37	3.767	0.385	0.60	1.77	1.18	376	212
124	SIR41	2.853	0.395	0.80	1.90	1.29	400	211

determined from in-place calibrations through the data recording system and the data reduction program. Propagation of the bias and of the precision errors through the calculated parameters[10] yielded the following uncertainties for the tunnel test conditions: p_{t1}, ±0.3 psia; T_{t1}, ±4°F; M_∞, ±0.03; and Re (per foot), ±1.32% of reading.

Data

The local heat transfer rates are presented as the dimensionless ratio h/h_{ref}. The heat transfer coefficient in the numerator is based on the measured heat transfer rate for the gauge of interest. The reference heat transfer rate used in the denominator was the equilibrium heat transfer rate to a sphere whose radius was 0.0175 ft, which is a 1-ft sphere reduced to the scale of the test model, as computed using the relations of Fay and Riddell.[11] Both for the numerator and for the denominator, the heat transfer coefficients were based on a recovery factor of 1. A statistical analysis of the data from several gauges was made (by personnel at AEDC) to determine the consistency of the data within a test run.[1] This procedure allowed one to account for data system noise and data reduction effects on the results. For heat transfer rates of 5.0 Btu/ft^{2}s, or more, the uncertainty is 7%; for heat transfer rates of 1.0 Btu/ft^{2}s, the uncertainty is 10%; and for heat transfer rates of 0.5 Btu/ft^{2}s, the uncertainty is 25%. For this analysis, the uncertainty represents two standard deviations, which includes 95% of the data. At the highest Reynolds number of the present tests, when the boundary layer was turbulent on the model at an angle of attack of 40 deg, the experimental values of the local heat transfer rate were as high as 15 Btu/ft^{2}s. At the lowest Reynolds number, when the boundary layer was laminar on the model at an angle of attack 35 deg, the experimental values of the local heat transfer rate were as low as 1.0 Btu/ft^{2}s.

Discussion of Results

Boundary-Layer Transition on the Smooth Model

As noted in a preceding section, an existing model was machined until the finish of the windward surface of the present MH-11 model was 0.0010 ± 0.0005 in. Because the model used in the present program as the reference smooth configuration (S1) was not really smooth, special runs were made to determine the transition locations for the reference smooth S1 model.

The onset of boundary-layer transition for the S1 model can be seen in the heat transfer distributions presented in Fig. 4 for an angle of attack of 40 deg. Note that, for every Reynolds number for which data were obtained, there is some x location on the model at which the experimental heat transfer coefficients begin to increase significantly above the values computed for a laminar boundary layer using the BLIMP code.[12] The departure of the measured heat transfer from the laminar theory is attributed to the onset of boundary-layer transition. Although the experimentally observed increase is relatively small for $ReL = 2.853$, the data nevertheless indicate the onset of boundary-layer transition at $x = 0.80L$ (see Ref. 7). Note that, as

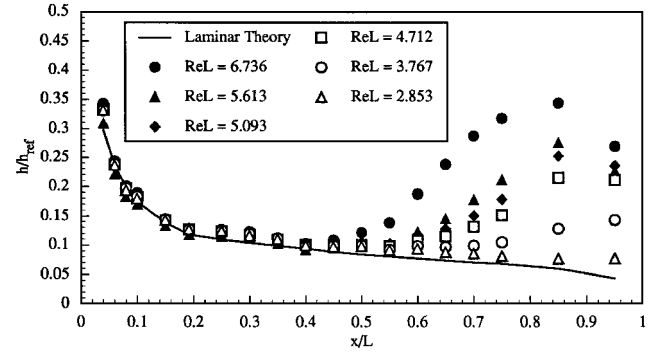

Fig. 4 Heat transfer distributions for the plane of symmetry of the smooth model (S1) at an angle of attack of 40 deg.

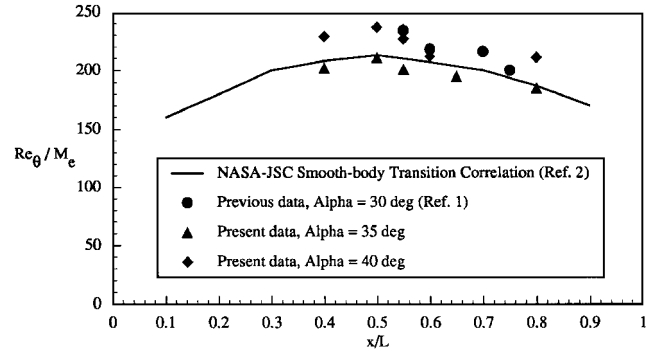

Fig. 5 Streamwise distribution of the Shuttle Orbiter transition correlation parameter (Re_θ/M_e).

would be expected, the onset of transition moves upstream toward the nose as the freestream Reynolds number increases. The peak and the subsequent decrease evident in the experimentally determined heat transfer distributions at the higher freestream Reynolds numbers indicate that the boundary layer near the aft end of the model is probably fully turbulent. The transition locations determined from the heat transfer distributions presented in Fig. 4 are summarized in Table 2. Also included in Table 2 are the values of transition-related parameters, such as Re_x, Re_θ, and Re_θ/M_e, evaluated at the point associated with the onset of boundary-layer transition. The reader may recall that the parameter Re_θ/M_e was commonly used in the preflight predictions for the onset of boundary-layer transition for the smooth Shuttle Orbiter.[2]

Values of the Shuttle Orbiter transition correlation parameter Re_θ/M_e are presented in Fig. 5. Data for $\alpha = 30$ deg from the previous OH4A test program[2] and for $\alpha = 35$ and 40 deg from the present program are compared with the JSC smooth-body transition

Table 3 Correlation parameters for boundary-layer transition with a roughness element in the windward pitch plane of the Shuttle Orbiter

Run	Configurations	ReL	T_w/T_t	x_{tr}/L	$(x_{tr}-x_{RE})L$	$Re_{k,RE}$	k/δ^*_{RE}	$(Re_\theta)_{RE}$	$(Re_\theta/M_e)_{RE}$
			Present data: $\alpha = 35$ deg; A-2 ($x_{RE} = 0.050L$, $k = 0.004$ in.)						
151	S3R3	4.698	0.396	0.050	0.000	209	2.32	85	88
			Present data: $\alpha = 35$ deg; G-3 ($x_{RE} = 0.375L$, $k = 0.015$ in.)						
63	S5R11	4.706	0.377	0.375	0.000	1439	2.43	317	162
66	S5R15	3.775	0.381	0.375	0.000	1107	2.08	285	145
69	S5R19	2.826	0.395	0.375	0.000	778	1.81	247	125
72	S5R23	1.918	0.416	0.375	0.000	446	1.37	199	102
73	S5R25	1.164	0.423	——[a]	W.L.	261	1.12	159	82
			Present data: $\alpha = 35$ deg; J-2 ($x_{RE} = 0.575L$, $k = 0.010$ in.)						
93	S10R3	4.712	0.387	0.575	0.000	807	1.19	445	205
95	S10R7	3.756	0.385	0.575	0.000	600	1.07	398	184
97	S10R11	2.769	0.397	0.575	0.000	397	0.90	344	159
100	S10R19	2.495	0.414	0.750	0.175	327	0.79	316	147
99	S10R15	1.909	0.417	W.L.	W.L.	221	0.69	280	130
			Present data: $\alpha = 40$ deg; A-2 ($x_{RE} = 0.050L$, $k = 0.004$ in.)						
150	S3R1	4.714	0.413	0.150	0.100	197	2.64	79	93
152	S3R5	3.785	0.399	0.400	0.350	155	2.32	71	84
153	S3R9	3.190	0.400	0.750–0.800	0.700–0.750	143	2.08	65	76
			Present data: $\alpha = 40$ deg; G-2 ($x_{RE} = 0.375L$, $k = 0.006$ in.)						
162	S5R5	3.814	0.397	0.375	0.000	263	0.94	262	166
163	S5R9	2.838	0.401	0.450	0.075	173	0.79	227	144
164	S5R15	2.344	0.405	W.L.[b]	W.L.	137	0.70	205	130

[a]Heat transfer was locally perturbed but quickly returned to the laminar level. [b]W.L. = wholly laminar.

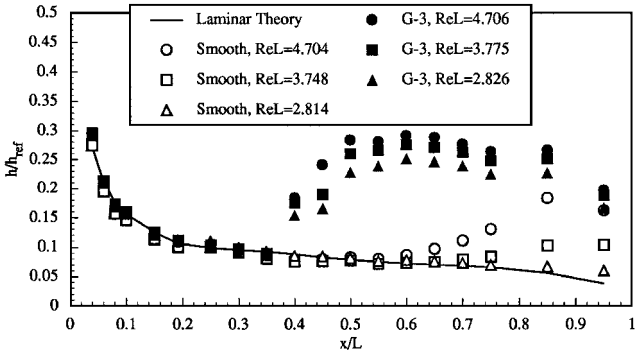

Fig. 6 Effect of the G-3 roughness element on the heat transfer distributions in the plane of symmetry with the S5 model at an angle of attack of 35 deg.

correlation.[2] The experimental values of Re_θ/M_e at the transition location for the S1 model of the present tests are in reasonable agreement both in magnitude and in the streamwise (or x) dependence with the experimental values from the previous program and with the JSC smooth-body transition correlation. The agreement exists despite the fact that the nominal surface finish of the smooth S1 configuration included 20% of the tiles misaligned as much as 0.0010 $\pm$ 0.0005 in. above the surrounding surface. In previous tests, the heat transfer distributions obtained on the MH2A model with 20% of the tiles (selected at random) misaligned by 0.0010 in. had a relatively small (albeit, measurable) effect on the boundary-layer transition location.[2,13] Because the smooth model in the present tests had a 1-mil distributed roughness, the boundary layer was probably perturbed, even though there was little or no movement of the experimentally determined onset of transition location.

Boundary-Layer Transition for Roughness Elements in the Plane of Symmetry

Heat transfer distributions were obtained with roughness elements located in the plane of symmetry at A, G, or J. At A, the roughness element was in a region where the inviscid local Mach number was just below 1 and there was a strong favorable pressure gradient. When the roughness element was at G or J, it was in a region where the local, inviscid Mach number was between 1.5 and 2.2 and the streamwise pressure gradient was relatively small. Thus, the roughness elements were in two very different environments.

The heat transfer distributions for the plane of symmetry of the Orbiter at an angle of attack of 35 deg are compared in Fig. 6 for the model with and without the G-3 roughness element (configuration S5). For the smooth model, boundary-layer transition occurs for all three test conditions, moving gradually upstream as the Reynolds number increases. However, for the same three Reynolds numbers, transition is fixed at the roughness element, i.e., $x = 0.375L$. Although the values of the transition parameter at the roughness element $(Re_\theta/M_e)_{RE}$ are in the range of 125–162 (significantly below the smooth-body correlation of Fig. 5), the values of the roughness Reynolds number at the roughness element $Re_{k,RE}$ are very high (in the range 778–1439). Thus, at these conditions, a 15-mil roughness element at G serves as an effective tripping device. Clearly, if the roughness Reynolds number is sufficiently high, a roughness element can serve as an effective tripping device in regions where the transition parameter (Re_θ/M_e) is relatively low. Recall that a roughness element is an effective tripping device if it causes boundary-layer transition to occur at a point just downstream of the element.

The heat transfer distributions from the plane of symmetry of the Orbiter at an angle of attack of 35 deg are presented in Fig. 7 for all five test conditions with the G-3 roughness element. Note that a significant increase in heat transfer occurs just downstream of the roughness element at every Reynolds number for which data were obtained. At the lowest Reynolds number for which data were obtained ($ReL = 1.164$), the heat transfer quickly returns to the laminar levels, indicating that boundary-layer transition did not occur. Referring to the roughness-related parameters presented in Table 3 for $ReL = 1.164$, $Re_{k,RE} = 261$, $k = 1.12\delta^*_{RE}$, and $(Re_\theta/M_e)_{RE} = 82$. Because the boundary-layer transition parameter is very low [in this case, $(Re_\theta/M_e)_{RE} = 82$], the roughness element apparently does not trip the boundary layer, despite the fact that $Re_{k,RE}$ is relatively high, i.e., 261. Thus, the boundary layer appears to be stable for these roughness-induced disturbances, and the heating quickly returns to the laminar level. For $ReL = 1.918$, while the roughness-induced flowfield perturbations produce a significant increase in heat transfer to the gauge at $x = 0.40L$, the heating pauses at $x = 0.45L$ before exhibiting the streamwise increase characteristic of a transitional boundary layer. Note that the heat transfer distribution in the transitional region is markedly different from that for the three higher Reynolds numbers. Nevertheless, transition for this run (run 72) is assumed to be fixed at the roughness element, resulting in the value of $(x_{tr} - x_{RE})/L = 0.000$ in Table 3.

The heat transfer measurements for configuration S5 at an angle of attack of 35 deg, when the Reynolds number was 4.706×10^6, are presented in Fig. 8 as the ratio $h_{rat,SS}$. The numerator of $h_{rat,SS}$ is the dimensionless heat transfer coefficient h/h_{ref} for the data obtained

on the configuration of interest at the freestream Reynolds number of interest; e.g., for Fig. 8, the configuration of interest (configuration S5 for these data) has the G-3 roughness element, and the freestream Reynolds number of interest is 4.706×10^6, or $ReL = 4.706$. The denominator for $h_{rat,SS}$ is the dimensionless heat transfer coefficient h/h_{ref} for the data obtained on the smooth configuration (S1) at the same freestream Reynolds number and at the same angle of attack of 35 deg. The use of data obtained on the smooth configuration at the same freestream Reynolds number for the denominator leads to the nomenclature SS in $h_{rat,SS}$. Note that the Reynolds number in the figure caption is that for the test conditions for the data in the numerator.

Thus, the ratio $h_{rat,SS}$ is a measure of the roughness-induced perturbation to the heat transfer. Values of $h_{rat,SS}$ less than 1.10 are considered within the experimental accuracy of the data and are represented by the open symbols at the heat transfer gauges. Consider the values of $h_{rat,SS}$ for $ReL = 4.706$, which are presented in Fig. 8. Most of the significant perturbations to the heat transfer are sensed by gauges in and near the plane of symmetry. Exceptions occur at three gauges near the wing root. The values of $h_{rat,SS}$ at these three gauges are 1.12, 1.13, and 1.20 (moving in the streamwise direction). If these perturbations are indeed significant, i.e., in excess of the run-to-run variations, they may be the result of interactions between the viscous/inviscid interactions associated with the wing-leading-edge flowfield.

The arrow that appears in Fig. 8 with the legend $x_{tr,s}$ indicates the location where boundary-layer transition occurred in the plane of symmetry of the smooth model at this (nominal) Reynolds number and angle of attack of 35 deg. Note that, for almost all of the heat transfer gauges located at, or downstream of, an x of $0.60L$, i.e., those gauges located in the wing area, boundary-layer transition has already produced convective heating rates to the smooth model well in excess of the laminar levels (see Ref. 6).

Heat transfer distributions from the plane of symmetry of the Orbiter model at an angle of attack of 40 deg are presented in Fig. 9 with the A-2 roughness element on the model. At the highest Reynolds number, i.e., $ReL = 4.714$, the roughness-induced flowfield perturbations produce a significant increase in heating immediately downstream of the roughness element. However, the strong favorable pressure gradient associated with the acceleration of the inviscid

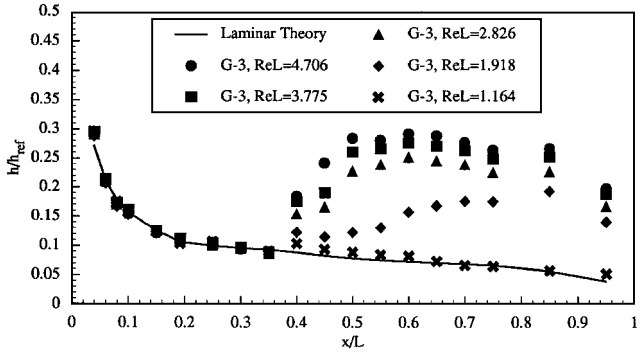

Fig. 7 Effect of the freestream Reynolds number on the plane-of-symmetry heat transfer distributions with the S5 model (G-3 roughness element) at an angle of attack of 35 deg.

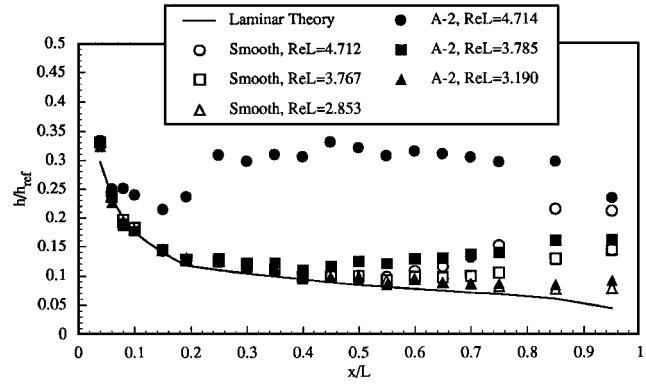

Fig. 9 Heat transfer distributions for the plane of symmetry of the S3 model (A-2 roughness element) at an angle of attack of 40 deg.

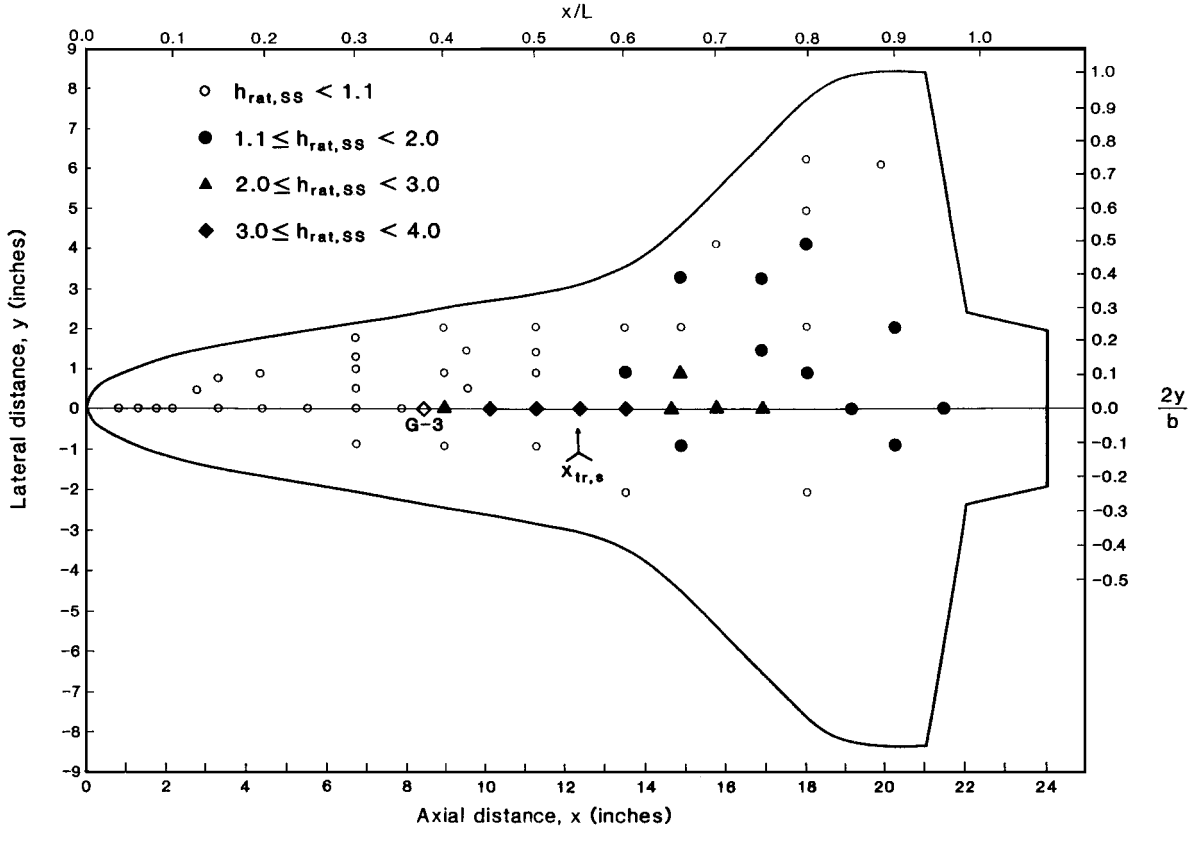

Fig. 8 Perturbed heating patterns on the S5 model (with the G-3 roughness element) at an angle of attack of 35 deg with $ReL = 4.706$.

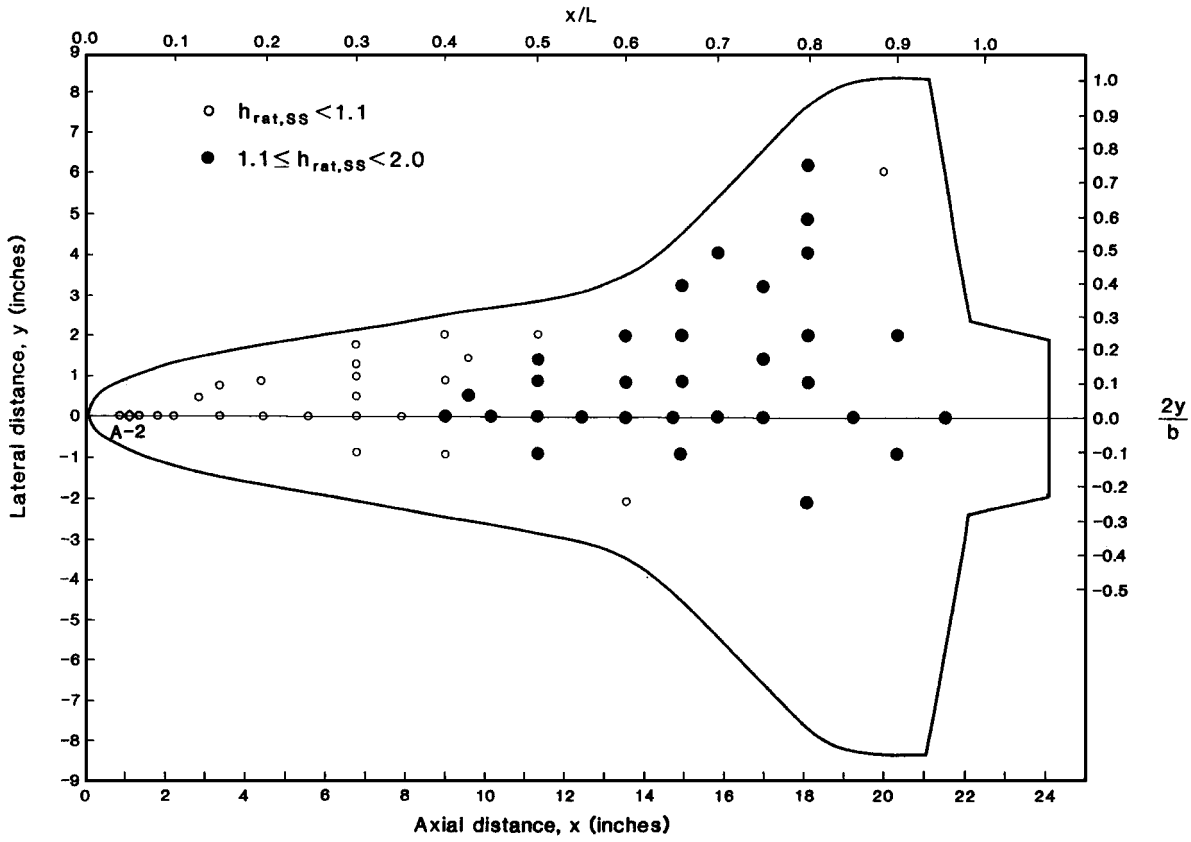

a) *ReL* = 3.785

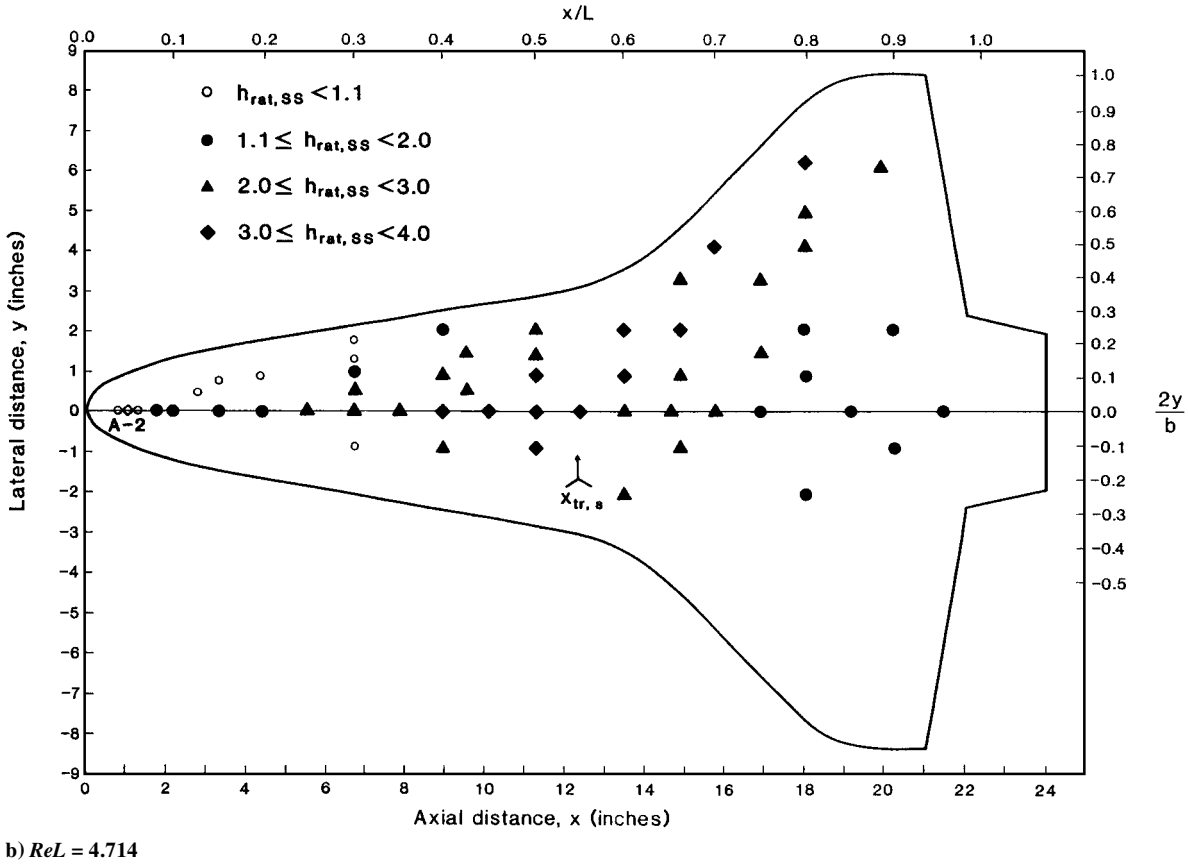

b) *ReL* = 4.714

Fig. 10 Perturbed heating patterns on the S3 model (with the A-2 roughness element) at an angle of attack of 40 deg.

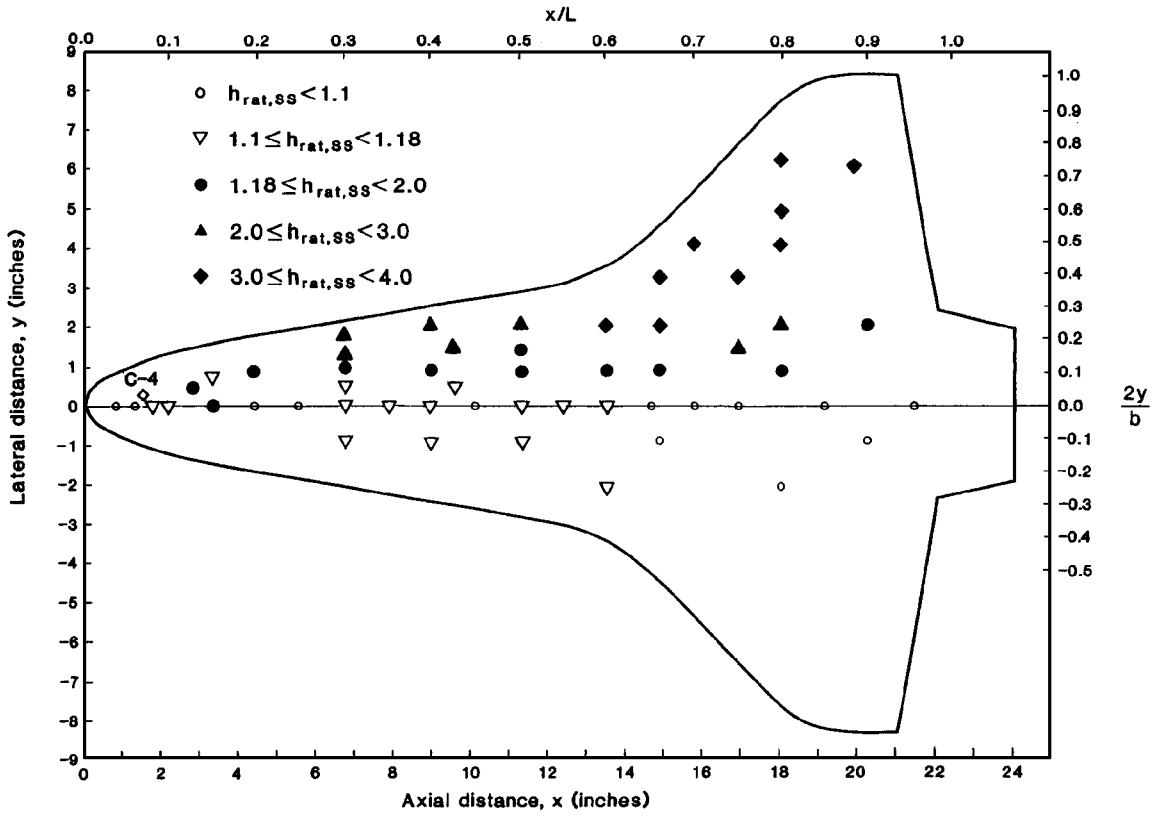

Fig. 11 Modified perturbed heating pattern on the S6 model (with the C-4 roughness element) at an angle of attack of 35 deg with $ReL = 3.779$.

flow in this region apparently attenuates the growth of turbulence in the region between $x = 0.080L$ and $0.150L$. From $x = 0.150L$, a rapid streamwise increase in the heating occurs, indicating the onset of boundary-layer transition. By $x = 0.250L$, the heat transfer has reached the fully turbulent level. Note that the roughness Reynolds number $Re_{k,\mathrm{RE}}$ for this run is 197 (Table 3) and is approximately the same as the effective value determined for the distributed misaligned tiles. Although the presence of the A-2 roughness element promotes transition for the two lower Reynolds number runs, transition is never fixed at the roughness element. The values of the roughness Reynolds number for these runs are 143 and 155 (Table 3).

The roughness-induced perturbations to the heat transfer at each of the gauges, as indicated by the values of the ratio $h_{\mathrm{rat,SS}}$, are presented in Fig. 10 for the A-2 configuration (S3) at an angle of attack of 40 deg. Despite the roughness-induced flowfield perturbations, transition does not occur until $x = 0.400L$ at a Reynolds number of $ReL = 3.785$. Although $k = 2.32\delta^*_{\mathrm{RE}}$, $Re_{k,\mathrm{RE}}$ is only 155, and $(Re_\theta/M_e)_{\mathrm{RE}}$ is only 84 (Table 3). Again, we have a case where the isolated roughness element is in a region where the boundary-layer transition parameters [in this case, $Re_{k,\mathrm{RE}}$ and $(Re_\theta/M_e)_{\mathrm{RE}}$] are very low. Another factor working against the roughness element at a promoting boundary-layer transition is that this roughness element is located where there is a strong favorable pressure gradient. Thus, although the roughness element produces locally high heating rates, it appears that the onset of transition is delayed. Referring to Table 2, the reader can see that transition would have occurred at $x = 0.60L$ on the smooth model at this Reynolds number. Nevertheless, once transition finally occurs, significant perturbations to the heat transfer spreads rapidly over most of the windward surface (Fig. 10a).

At the higher Reynolds number, i.e., $ReL = 4.714$, the roughness-induced perturbations spread over most of the windward surface. The data presented in Fig. 10b indicate that not only did the presence of the A-2 roughness element in the subsonic flowfield at the nose of the model move transition well upstream but also the presence of this roughness element in a region where many of the streamlines for the windward surface originate also produced significant roughness-induced heat transfer perturbations at virtually every heat transfer gauge on the windward surface. Vortices shed from the A-2 roughness element create a complex pattern of heat transfer perturbations, as can be seen by locating the heat transfer gauges where $h_{\mathrm{rat,SS}}$ exceeds 3.0, which are distributed over the windward surface (Fig. 10b).

Boundary-Layer Transition for Roughness Elements off the Plane of Symmetry

The ratio $h_{\mathrm{rat,SS}}$, which is a measure of the roughness-induced perturbation to the heat transfer at a given gauge, is presented in Fig. 11 for the C-4 roughness element (configuration S6) with the model at an angle of attack of 35 deg. Values of $h_{\mathrm{rat,SS}}$ are presented for a freestream Reynolds number based on model length of ReL equal to 3.779. The filled symbols that represent significant roughness-induced perturbations to the heat transfer at a specific gauge assume a threshold value for $h_{\mathrm{rat,SS}}$ of 1.18. The use of 1.18 as the threshold value of $h_{\mathrm{rat,SS}}$ (instead of 1.10, as was done for Figs. 8 and 10) would imply that the data for the numerator were on the plus side of the experimental uncertainty, whereas those for the denominator were on the minus side of the experimental uncertainty. Reviewing the more complete data presented in Ref. 6, one would see that the experimental values of h/h_{ref} at this ReL were the lowest of any of the 35-deg-angle-of-attack smooth-model measurements over the entire range of Reynolds numbers tested. Thus, the smooth-model measurements that constitute the denominator of $h_{\mathrm{rat,SS}}$ were indeed on the minus side of the experimental uncertainty. Therefore, the use of a threshold value for $h_{\mathrm{rat,SS}}$ of 1.18 seems to be more representative of the significant roughness-induced perturbations for these data. Heat transfer gauges for which $h_{\mathrm{rat,SS}}$ was between 1.10 and 1.18 are indicated by an open, inverted triangle. For either assumption for the threshold value of $h_{\mathrm{rat,SS}}$, the presence of the C-4 roughness element produces increased heating over roughly one-half of the model, moving the onset of boundary-layer transition so that it is fixed at the roughness. The roughness-related transition parameters are presented in Table 4. Although the value of $(Re_\theta/M_e)_{\mathrm{RE}}$ is only 87, the value of $Re_{k,\mathrm{RE}}$ of 692 is apparently above the effective value for the roughness Reynolds number.

Values of $h_{\mathrm{rat,SS}}$, the roughness-induced heat transfer perturbation, are presented in Fig. 12 for configuration S11, i.e., that with the F-3 roughness element, at an angle of attack of 35 deg with $ReL = 2.830$. The values of $h_{\mathrm{rat,SS}}$ indicate that, at this relatively

Table 4 Correlation parameters for boundary-layer transition with a roughness element away from the windward pitch plane of the Shuttle Orbiter

Run	Configurations	ReL	T_w/T_t	Transition location[a]	$Re_{k,\mathrm{RE}}$	$(Re_\theta)_{\mathrm{RE}}$	$(Re_\theta/M_e)_{\mathrm{RE}}$
		Present data: $\alpha = 35$ deg; F-3 ($x_{RE} = 0.258L$, $2y_{RE} = 0.107b$, $k = 0.015$ in.)					
156	S11R3	4.706	0.377	F.A.R.	1200	257	143
158	S11R7	3.747	0.382	F.A.R.	919	230	128
159	S11R17	3.308	0.382	Transitional	800	216	120
161	S11R11	2.830	0.351	Transitional	650	198	110
		Present data: $\alpha = 35$ deg; K-3 ($x_{RE} = 0.620L$, $2y_{RE} = 0.366b$, $k = 0.008$ in.)					
93	S10R3	4.712	0.387	F.A.R.	769	338	165
95	S10R7	3.756	0.385	F.A.R.	566	301	147
97	S10R11	2.769	0.397	F.A.R.	368	260	127
100	S10R19	2.495	0.414	F.A.R.	300	240	117
99	S10R15	1.909	0.417	W.L.	200	213	104
		Present data: $\alpha = 35$ deg; C-4 ($x_{RE} = 0.070L$, $2y_{RE} = 0.030b$, $k = 0.015$ in.)					
139	S6R3	3.771	0.376	F.A.R.	692	101	87
144	S6R25	3.779	0.390	F.A.R.	692	101	87
142	S6R7	2.844	0.397	F.A.R.	510	87	74
		Present data: $\alpha = 35$ deg; C-3 ($x_{RE} = 0.070L$, $2y_{RE} = 0.030b$, $k = 0.008$ in.)					
80	S6R9	3.782	0.374	F.A.R.	368	101	87
82	S6R5	2.846	0.388	Transitional	267	87	74
83	S6R11	2.804	0.389	Transitional	267	87	74
85	S6R13	1.915	0.408	W.L.	170	70	60
		Present data: $\alpha = 40$ deg; F-3 ($x_{RE} = 0.258L$, $2y_{RE} = 0.107b$, $k = 0.015$ in.)					
155	S11R1	4.709	0.378	F.A.R.	1054	240	162
157	S11R5	3.781	0.381	F.A.R.	822	215	145
160	S11R9	2.763	0.392	F.A.R.	589	185	125
		Present data: $\alpha = 40$ deg; C-4 ($x_{RE} = 0.070L$, $2y_{RE} = 0.030b$, $k = 0.015$ in.)					
138	S6R1	3.748	0.370	F.A.R.	638	92	92
143	S6R23	3.795	0.391	F.A.R.	638	92	92
141	S6R25	2.820	0.390	W.L.	478	80	80
		Present data: $\alpha = 40$ deg; E-2 ($x_{RE} = 0.258L$, $2y_{RE} = 0.043b$, $k = 0.005$ in.)					
28	S2R1	4.696	0.411	W.L.	237	170	149
29	S2R3	3.782	0.414	W.L.	180	150	132
30	S2R5	2.780	0.416	W.L.	120	130	114
31	S3R7	1.896	0.440	W.L.	66	107	94
		Present data: $\alpha = 40$ deg; I-2 ($x_{RE} = 0.375L$, $2y_{RE} = 0.146b$, $k = 0.006$ in.)					
28	S2R1	4.696	0.411	F.A.R.	350	228	170
29	S2R3	3.782	0.414	Transitional	267	205	153
30	S2R5	2.780	0.416	W.L.	177	176	131
31	S3R7	1.896	0.440	W.L.	100	143	107

[a]F.A.R. = fixed at roughness, Transitional = transition occurs between the roughness element and the end of the model, and W.L. = wholly laminar.

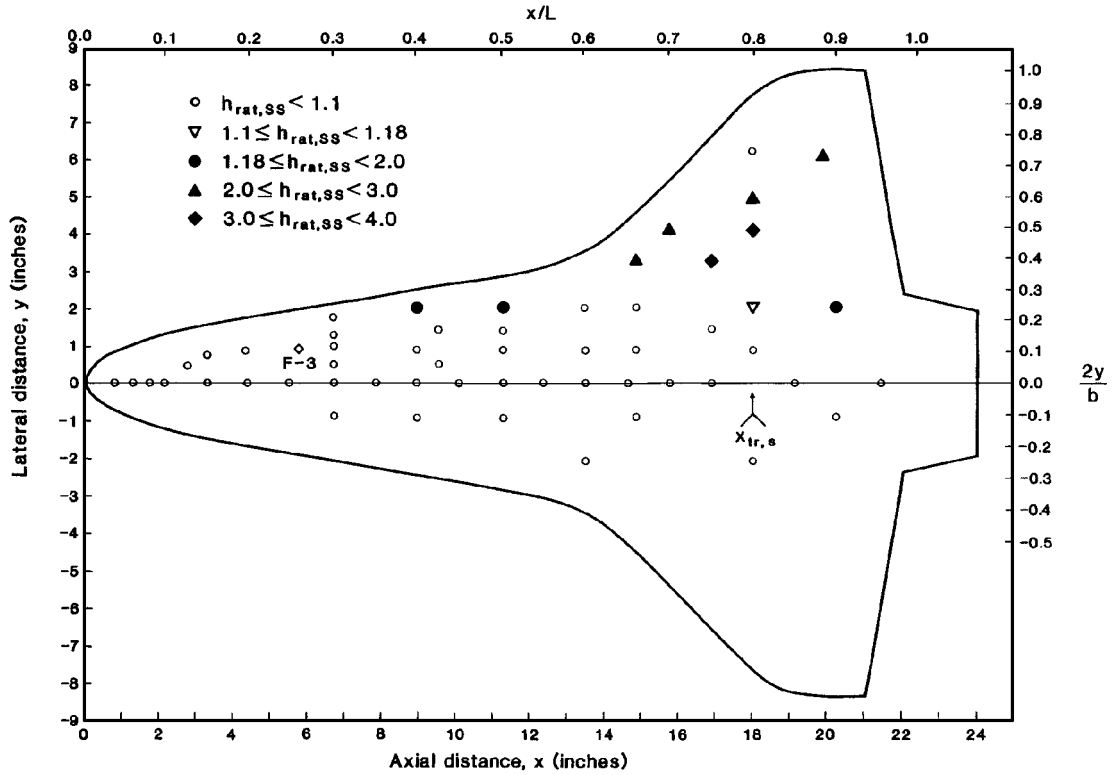

Fig. 12 Perturbed heating pattern on the S11 model (with the F-3 roughness element) at an angle of attack of 35 deg with $ReL = 2.830$.

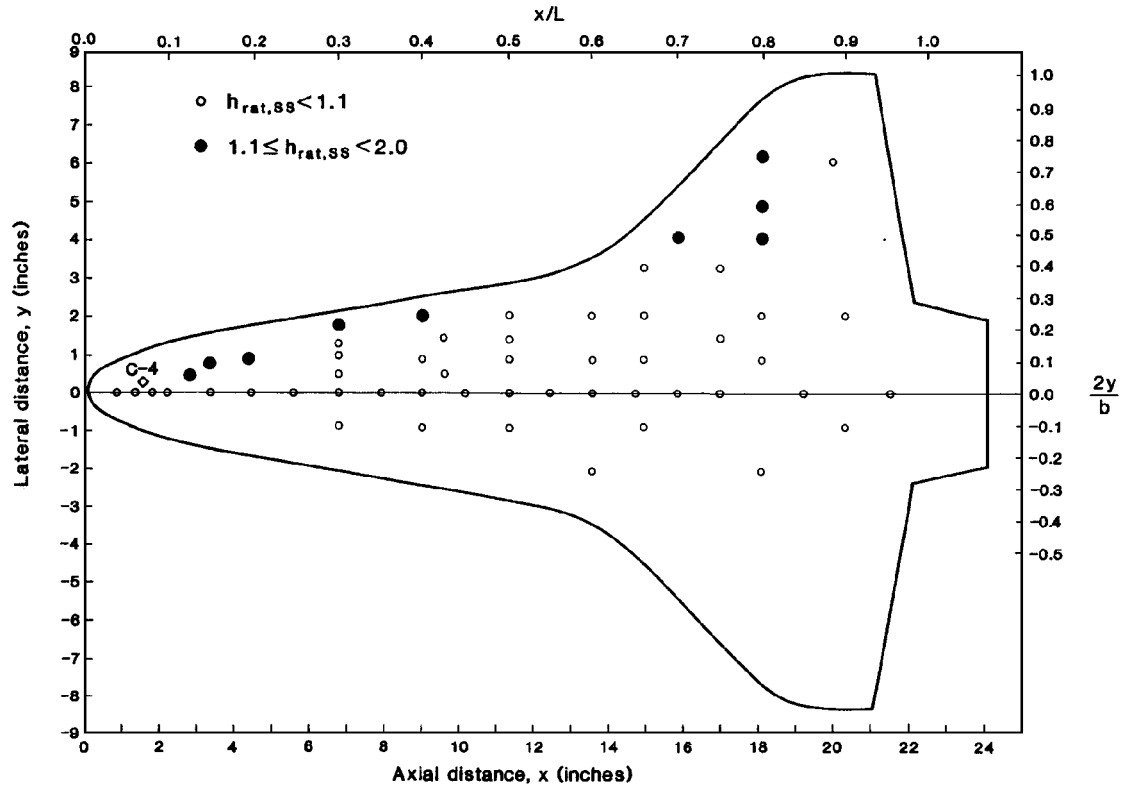

Fig. 13 Perturbed heating pattern on the S6 model (with the C-4 roughness element) at an angle of attack of 40 deg with $ReL = 3.748$.

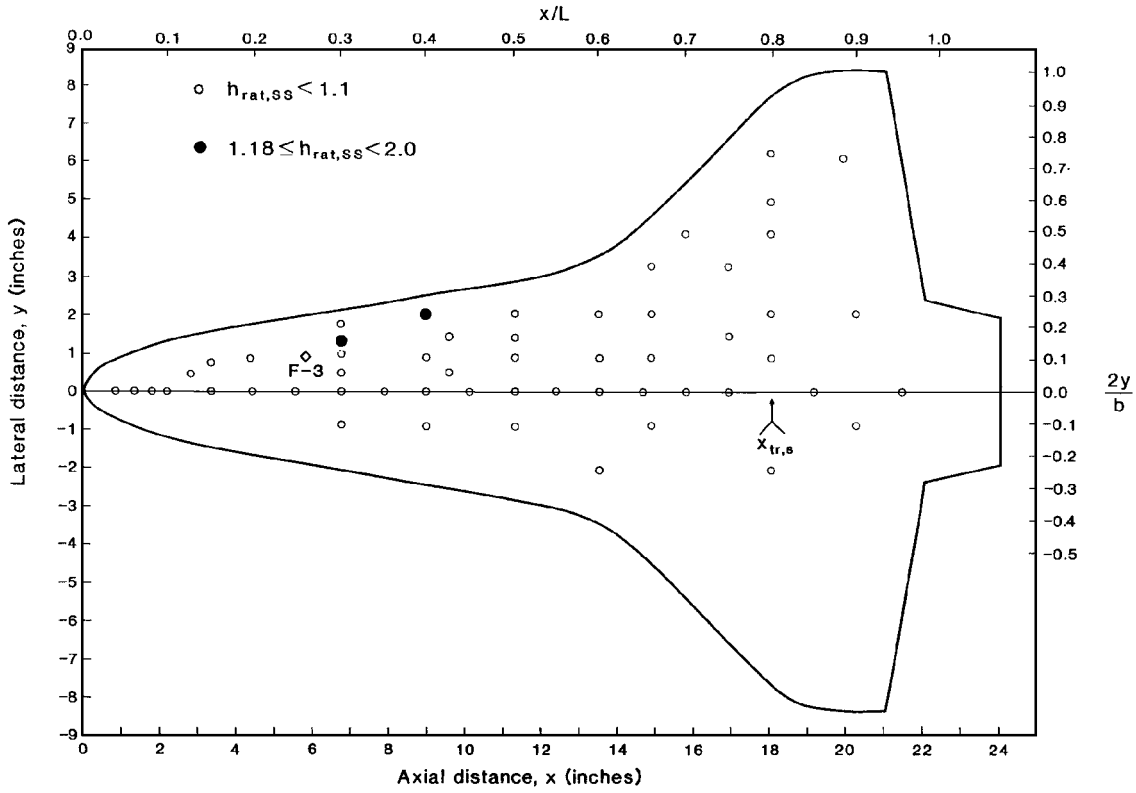

Fig. 14 Perturbed heating pattern on the S11 model (with the F-3 roughness element) at an angle of attack of 40 deg with $ReL = 2.763$.

low Reynolds number, the flow is transitional due to the roughness-induced flowfield perturbations. The value of the transition parameter at the roughness element $(Re_\theta/M_e)_{\mathrm{RE}}$ is only 110 (Table 4). Thus, although the $Re_{k,\mathrm{RE}}$ value of 650 actually exceeds the effective values of $Re_{k,\mathrm{RE}}$ for most of the other test conditions, the onset of boundary-layer transition does not seem to occur until the wing. The surface area affected by the roughness-induced perturbations roughly follows a streamline on the fuselage before spreading out over the wing, with the affected area on the wing increasing as the Reynolds number increases. At the highest Reynolds number ($ReL = 4.706$), all of the gauges on the wing, including those on the opposite side of the plane of symmetry, i.e., those at negative values of y, experience increased heating.[6]

Values of $h_{\mathrm{rat,SS}}$ are presented for configuration S6 (that with the C-4 roughness element) and for configuration S11 (that with the F-3 roughness element) for an angle of attack of 40 deg in Figs. 13 and 14, respectively. For the data presented in Figs. 13 and 14, boundary-layer transition appears to be fixed at the roughness. See

Table 4 for the roughness-related transition parameters. Configuration S6 (with the C-4 roughness element) at an angle of attack of 40 deg is the only one for which the off-plane-of-symmetry roughness element was in a region where the inviscid flow was transonic (because M_e is 0.995 at this roughness element). Referring to Table 4, the boundary layer remains laminar at the lowest Reynolds number tested ($ReL = 2.820$) despite the roughness-induced perturbations for this flow where $(Re_\theta/M_e)_{RE}$ is 80 and $Re_{k,RE}$ is 478. The reader should compare these values with those presented in Table 3 for the roughness elements in the subsonic region of the plane of symmetry.

The reader should compare the patterns of roughness-induced perturbations to the heat transfer when the model is at an angle of attack of 40 deg, as presented in Figs. 13 and 14, with the patterns when the model is at an angle of attack of 35 deg, as presented in Figs. 11 and 12. At 40-deg angle of attack, only a relatively small surface area experiences significant increases in the heat transfer due to the presence of the roughness element, as indicated by values of $h_{rat,SS}$ in excess of 1.10, i.e., the filled symbols of Figs. 13 and 14. In fact, it appears that the perturbations due to the F-3 roughness are quickly swept off the windward surface. As discussed in a preceding section about the model and as can be seen in Figs. 2 and 3, roughness elements C and F are located near (even outboard of) the attachment line, when the model is at an angle of attack of 40 deg.

Concluding Remarks

Based on the analysis of the data from the present tests, the following conclusions are made.

1) The present data for the smooth model exhibited the same streamwise dependence on the Shuttle Orbiter transition correlation as did the earlier tests. The region of increased heating due to the onset of boundary-layer transition not only moved upstream as the freestream Reynolds number increased but also spread outward away from the plane of symmetry. An oval, horseshoe-like pattern occurred. The greatest heating occurred in the plane of symmetry.

2) For the smooth model and for the models with discrete roughness elements in the plane of symmetry, the measurements for $\alpha = 35$ deg exhibited trends similar to those for $\alpha = 40$ deg. However, when the roughness element was located away from the plane of symmetry, the surface area affected by roughness-induced perturbations to the heat transfer was sensitive to the angle of attack.

3) For the present tests, Re_θ, Re_θ/M_e, and Re_k were found to be the most useful correlation parameters. Correlations using roughness height relative to parameters associated with the boundary-layer thickness, e.g., k/δ, k/δ^*, and k/θ, failed to provide consistent results. Correlations developed using the data for the discrete roughness elements of the present tests were found to be similar to correlations for distributed roughness elements as reported by Bertin et al.[2] Of course, in addition to the presence of discrete (isolated) roughness elements on the model, there was a residual background, distributed roughness of 0.0010 in. Thus, in reality, the flowfield perturbations produced by the discrete roughness were probably assisted by the background distributed roughness to produce the observed boundary-layer transition. The interested reader is referred to Ref. 6 for a discussion of the data that support this conclusion.

4) There was no evidence that the presence of a roughness element near the attachment line was more likely to promote the onset of transition than was the presence of a roughness element in the plane of symmetry. In fact, the transition correlations with a roughness element in the plane of symmetry were usually similar to those with a roughness element near the attachment line. The roughness-induced transition correlations depended on both $Re_{k,RE}$ and $(Re_\theta/M_e)_{RE}$.

5) Not only did the presence of the A-2 roughness element in the subsonic region of the nose move transition well upstream but also significant roughness-induced heat transfer perturbations occurred at nearly every heat transfer gauge on the windward surface at the highest Reynolds number. Vortices shed from the roughness element produced a complex pattern of perturbed heating.

Acknowledgment

The authors would like to thank Tim C. Valdez for his help in preparing many of the figures presented in this paper.

References

[1] Martindale, W. R., and Trimmer, L. L., "Test Results from the NASA/Rockwell International Space Shuttle Test (OH4A) Conducted in the VKF Tunnel B," Arnold Engineering Development Center, AEDC-DR-74-39, Arnold Air Force Station, TN, May 1974.

[2] Bertin, J. J., Hayden, T. E., and Goodrich, W. D., "Shuttle Boundary-Layer Transition Due to Distributed Roughness and Surface Cooling," *Journal of Spacecraft and Rockets*, Vol. 19, No. 5, 1982, pp. 389–396.

[3] Goodrich, W. D., Derry, S. M., and Bertin, J. J., "Shuttle Orbiter Boundary Layer Transition at Flight and Wind Tunnel Conditions," *Shuttle Performance: Lessons Learned*, NASA CP 2283, Pt. 2, March 1983.

[4] Bouslog, S. A., Bertin, J. J., Berry, S. A., and Caram, J. M., "Isolated Roughness Induced Boundary-Layer Transition: Shuttle Orbiter Ground Tests and Flight Experience," AIAA Paper 97-0274, Jan. 1997.

[5] Bouslog, S. A., An, M. Y., Hartmann, L. N., and Derry, S. M., "Review of Boundary Layer Transition on the Space Shuttle Orbiter," AIAA Paper 91-0741, Jan. 1991.

[6] Bertin, J. J., and Stetson, K. F., "The Effect of Surface Roughness on Shuttle Orbiter Boundary-Layer Transition," Lockheed Martin Engineering and Science Services, LMES-32017, Houston, TX, Jan. 1996.

[7] Bertin, J. J., Stetson, K. F., Bouslog, S. A., and Caram, J. M., "Effect of Isolated Roughness Elements on Boundary-Layer Transition for Shuttle Orbiter," AIAA Paper 96-1906, June 1996.

[8] An, M. Y., Wang, K. C., and Tam, L. T., "Computation of Inviscid Flowfield Around 3-D Aerospace Vehicles and Comparison with Experimental and Flight Data," AIAA Paper 93-0885, Jan. 1993.

[9] Gnoffo, P., and Weilmuenster, K., "A Multiblock Analysis for Shuttle Orbiter Re-Entry Heating from Mach 24 to Mach 12," AIAA Paper 93-2813, July 1993.

[10] Nutt, K. W., "Space Shuttle Orbiter Boundary-Layer Transition Test (MH-11) in AEDC Tunnel B (Mach 8)," Arnold Engineering Development Center, AEDC-TSR-95-V4, Arnold Air Force Station, TN, Oct. 1995.

[11] Fay, J. A., and Riddell, F. R., "Theory of Stagnation Point Heat Transfer in Dissociated Air," *Journal of the Aeronautical Sciences*, Vol. 25, No. 2, 1958, pp. 73–85.

[12] Tong, H., Buckingham, A. C., and Morse, H. L., "Nonequilibrium Chemistry Boundary Layer Integral Matrix Procedure," Acurex Corp. Aerotherm Final Rept. 73-67, Mountain View, CA, July 1973.

[13] Bertin, J. J., Idar, E. S., III, and Goodrich, W. D., "Effect of Surface Cooling and Roughness on Transition for the Shuttle Orbiter," *Journal of Spacecraft and Rockets*, Vol. 15, No. 2, 1978, pp. 113–119.

J. C. Adams Jr.
Associate Editor